VERTEX-BASED PRECONDITIONERS FOR THE COARSE PROBLEMS OF BDDC

CLARK R. DOHRMANN*, KENDALL H. PIERSON*, AND OLOF B. WIDLUND†

TR2019-993

Abstract. We present a family of approximate BDDC preconditioners based on inexact solvers for the coarse problem. The basic idea is to replace the direct solver for a standard BDDC coarse problem by a preconditioner which requires much less computation and memory. The focus in this study is on scalar elliptic and linear elasticity problems in three dimensions. The preconditioner for the coarse problem employs a standard two-level additive Schwarz approach in which the coarse problem dimension is either one or six times the number of subdomain vertices. We show, under certain assumptions on the coefficients, that favorable BDDC condition number estimates also hold for the approximate preconditioners. Numerical examples are presented to confirm the theory and to demonstrate the computational advantages of the approach.

Key words. elliptic equations, linear elasticity, finite elements, domain decomposition methods, BDDC algorithms, small coarse spaces,

AMS subject classifications. 65F08, 65F10, 65N30, 65N55

1. Introduction.

In this study, we present approximate Balancing Domain Decomposition by Constraints (BDDC) preconditioners for three-dimensional scalar elliptic and linear elasticity problems in which the direct solution of the coarse problem is replaced by a preconditioner based on a smaller vertex-based coarse space. By doing so, the computational and memory requirements can be reduced significantly. Although the use of standard coarse spaces based on subdomain vertices (corners) alone has similar memory benefits, the associated rate of convergence is not attractive as the number of elements per subdomain grows, cf. e.g. [17]. This point is illustrated by a simple motivating example in the next section.

There exists a rich theory for Finite Element Tearing and Interconnecting Dual Primal (FETI-DP) and BDDC algorithms for scalar elliptic and linear elasticity problems in three dimensions; see, e.g., [17], [19] and [28, Section 6.4.2]. In many cases, theoretical results for either FETI-DP or BDDC apply directly to the other because the eigenvalues of the preconditioned operators differ by at most two, see [24, 21, 2]. This result does not hold in the present study because the basic FETI-DP algorithm [11] is not easily adapted to the use of a preconditioner instead of a direct solver for the symmetric and positive definite coarse problem. In contrast, such a change is accommodated easily by BDDC in both theory and practice, see [7].

Our approach to precondition the BDDC coarse problem is motivated in part by more recent developments of small coarse spaces for domain decomposition algorithms [8]; see also [13]. Although that study was focused on overlapping Schwarz methods, similar ideas can be used to construct coarse spaces for preconditioning the BDDC coarse problem. Compared with larger edge- or face-based

*Computational Solid Mechanics and Structural Dynamics Department, Sandia National Laboratories, Albuquerque, New Mexico, 87185 crdohrm@sandia.gov, khpiers@sandia.gov. Sandia National Laboratories is a multimission laboratory managed and operated by National Technology and Engineering Solutions of Sandia, LLC., a wholly owned subsidiary of Honeywell International, Inc., for the U.S. Department of Energy's National Nuclear Security Administration under Contract DE-NA0003525. This research was supported by the Exascale Computing Project (17-SC-20-SC), a collaborative effort of two U.S. Department of Energy organizations (Office of Science and the National Nuclear Security Administration) responsible for the planning and preparation of a capable exascale ecosystem, including software, applications, hardware, advanced system engineering, and early testbed platforms, in support of the nations exascale computing imperative.

†Courant Institute of Mathematical Sciences, 251 Mercer Street, New York, NY 10012, USA widlund@cims.nyu.edu, http://cs.nyu.edu/cs/faculty/widlund/index.html. The work of this author was supported in part by the National Science Foundation Grant DMS-1522736.

coarse spaces, we show that similar condition number bounds can be achieved at lower cost under certain assumptions on material property jumps between adjacent subdomains.

We note that three- and multi-level BDDC algorithms [29, 30, 25] can also be viewed as using an inexact solver for the coarse problem, but such approaches are fundamentally different from ours. Namely, those algorithms construct and apply (recursively for multilevel approaches) a BDDC preconditioner for the original two-level coarse problem. In contrast, we do not introduce additional coarse levels and instead make use of standard two-level additive Schwarz concepts for preconditioning of the coarse problem. One important result of using smaller coarse spaces is that larger numbers of subdomains are feasible before needing to use a three- or multi-level approach. Consequently, the number of coarse levels can potentially be reduced resulting in fewer synchronization points. We also note that approximate solvers of the coarse problem were introduced in [15] in the context of a saddle-point formulation for FETI-DP. Successful approximate solvers for coarse FETI-DP components, based on an algebraic multigrid algorithm, have also been developed in [16]. For recent work on multi-level FETI–DP algorithms, see [27].

Reducing the size of the coarse problem while retaining favorable convergence rates was also the subject of Algorithm D in [17]. The basic idea there was to use a coarse space based on a subset of subdomain edges and corners (vertices) rather than all of them. The authors note that their recipe for selecting such edges and corners is relatively complicated, but this approach can effectively reduce the coarse problem dimension. This was followed by a study of compressible elasticity [19]; its final subsection outlines a strategy of constructing a minimal coarse space for the FETI-DP algorithm. We note that these results depend on the assumption that the coefficients in the subdomains are constant and that their values can be used when designing this component of the preconditioner. In contrast to that work, the present algorithms use coarse space variables related to all subdomain edges or all subdomain faces, but replace the direct solver for the coarse problem with a preconditioner.

A motivating example is presented in the next section for the proposed approach, which is summarized in §3. Some auxiliary results are developed in §3.1. Of particular importance is the use of [30, Lemma 4.2] and an analog thereof, developed in this paper, for algorithms based on subdomain faces. This is then followed in §4 by the analysis, which provides our main theoretical results for the scalar case, and by an analysis for linear elasticity in §5. The final two sections of the paper deal with implementation details and numerical results which confirm the theory and demonstrate the computational advantages of the approach.

2. Motivation. To help motivate the proposed approach, consider a unit cube domain partitioned into 27 smaller cubic subdomains. Each of these subdomains is discretized using H/h lowest order hexahedral elements in each coordinate direction for the Poisson equation with constant material properties. Homogeneous essential boundary conditions are applied to one face of the unit cube and a random load vector b is used for the linear system $Ax = b$. We note that in our algorithm, we solve the interface problem $Su_\Gamma = g$ by iteration after eliminating the residuals in the subdomain interiors in an initial static condensation step. Here, S is the Schur complement matrix associated with the remaining interface variables.

We first consider coarse spaces based on subdomain vertices alone or edges alone. Table 2.1 shows the condition number estimates for the preconditioned operator along with the number of iterations needed to achieve a relative residual tolerance of 10^{-8} using the conjugate gradient algorithm preconditioned using BDDC. The fast growth of condition numbers in the third column is consistent with a bound proportional to $(H/h)(1 + \log(H/h))^2$ as given in [17, Remark 2]. The shortcomings of using coarse spaces based on vertices alone were also recognized early in the history of FETI-DP, cf. [10]. We note that the results for the proposed approach show significant improvements in comparison to the standard vertex (corner) based coarse space.

Results are also shown in Table 2.2 for an increasing numbers of subdomains N and fixed

TABLE 2.1
Poisson equation results. Number of iterations (iter) and condition number estimates (cond) are shown for a unit cube domain constrained on one side and decomposed into 27 smaller cubic subdomains.

	standard approach				proposed approach	
	vertices		edges			
H/h	iter	cond	iter	cond	iter	cond
4	28	27.1	12	2.36	14	2.50
8	38	75.2	14	2.93	16	3.13
12	45	132	16	3.37	18	3.59
16	47	195	17	3.73	19	3.97

TABLE 2.2
Poisson equation results. Coarse space dimension n_c and convergence results are shown for increasing numbers of subdomains N and fixed $H/h = 8$.

	standard approach						proposed approach		
	vertices			edges					
N	n_c	iter	cond	n_c	iter	cond	n_c	iter	cond
64	27	55	74.5	108	15	2.98	27	17	3.25
216	125	70	73.7	450	15	2.94	125	17	3.26
512	343	74	73.6	1176	15	2.95	343	17	3.30
1000	729	75	73.6	2430	15	2.95	729	17	3.32

$H/h = 8$. We note that the dimensions n_c of the coarse space for edge-based coarse spaces are significantly larger than those for the proposed approach. Again, the advantages of the new approach are evident in the final three columns of the table where the numbers of iterations and condition numbers are much smaller than those for the standard vertex-based coarse space.

One of the primary goals of this study is to present an approach that has the best of both worlds. That is, an approach that has the attractive convergence rates of edge or face-based coarse spaces and the more streamlined computational requirements of a smaller vertex-based coarse space.

3. Overview of BDDC and Approach. We will first focus our analysis on the scalar elliptic problem: find $u \in H_0^1(\Omega)$ such that

$$a(u,v) = f(v) \quad \forall v \in H_0^1(\Omega, \partial\Omega),$$

where

$$H_0^1(\Omega) := \{v \in H^1(\Omega) : v = 0 \ \ on \ \ \partial\Omega\},$$

and

$$a(u,v) := \int_\Omega \rho(x) \nabla u \cdot \nabla v dx, \qquad f(v) := \int_\Omega f v dx.$$

The diffusion coefficient $\rho(x) > 0$ is assumed to take on a constant value in each subdomain when we develop our theory. We will consider finite element approximations of u based on lowest order tetrahedral or hexahedral elements.

We could equally well develop our algorithm for the case when part of $\partial\Omega$ is subject to a Neumann boundary condition and we will do so when considering the equations of elasticity.

The domain Ω for the problem is assumed to be partitioned into nonoverlapping subdomains $\Omega_1, \ldots, \Omega_N$. The set of interface nodes that are common to two or more subdomain boundaries is denoted by Γ, and the set of those on $\partial\Omega_i$ is denoted by $\Gamma_i := \Gamma \cap \partial\Omega_i$. The constant value of $\rho(x)$ in Ω_i is denoted by ρ_i. The finite element nodes on Γ_i are partitioned into equivalence classes

associated with subdomain vertices, edges, or faces and are defined in terms of the indices of the subdomains with boundaries to which they belong; see, e.g., [6] or [8] for more details.

A two-level BDDC preconditioner, see, e.g. [6], can be expressed concisely in additive form as

$$M^{-1} = M_{local}^{-1} + \Phi_D K_c^{-1} \Phi_D^T, \tag{3.1}$$

where K_c is the coarse matrix and Φ_D is a weighted interpolation matrix. We note that application of the local component M_{local}^{-1} requires solutions of problems local to each subdomain, which can be done in parallel.

The coarse matrix is obtained from the assembly of coarse subdomain matrices and is given by

$$K_c = \sum_{i=1}^{N} R_{ic}^T K_{ic} R_{ic},$$

where K_{ic} is the contribution of Ω_i to the coarse matrix and $u_{ic} = R_{ic} u_c$ the restriction of a coarse vector u_c to Γ_i. Let M_c^{-1} denote a preconditioner for K_c which satisfies the bounds

$$\beta_1 u_c^T K_c^{-1} u_c \leq u_c^T M_c^{-1} u_c \leq \beta_2 u_c^T K_c^{-1} u_c \quad \forall u_c, \tag{3.2}$$

where $0 < \beta_1 \leq \beta_2$. Defining the approximate BDDC preconditioner M_a^{-1} as

$$M_a^{-1} := M_{local}^{-1} + \Phi_D M_c^{-1} \Phi_D^T,$$

we find from (3.1) and (3.2) that

$$\begin{aligned} p^T M_a^{-1} p &= p^T (M^{-1} + \Phi_D (M_c^{-1} - K_c^{-1}) \Phi_D^T) p \\ &\leq p^T (M^{-1} + (\beta_2 - 1) \Phi_D K_c^{-1} \Phi_D^T) p \\ &\leq \max(1, \beta_2) p^T M^{-1} p. \end{aligned} \tag{3.3}$$

Similarly,

$$p^T M_a^{-1} p \geq \min(1, \beta_1) p^T M^{-1} p. \tag{3.4}$$

Let κ denote the condition number of the originating BDDC preconditioned operator. It then follows from (3.3) and (3.4) that

$$\kappa_a \leq \frac{\max(1, \beta_2)}{\min(1, \beta_1)} \kappa, \tag{3.5}$$

where κ_a is the condition number of the approximate BDDC preconditioned operator. Here we only consider preconditioners for the coarse matrix K_c, but approximations for other components of the BDDC preconditioner have also been studied in [7, 22].

The construction of the preconditioner M_c^{-1} for K_c was inspired in part by our recent work on small coarse spaces [8]. What we here, thus far, have called vertices are generalized there and called coarse nodes. We recall that the coarse degrees of freedom for BDDC or FETI-DP are often associated with average values over the different equivalence classes. The basic idea of the coarse component of our preconditioner M_c^{-1} is to approximate these averages using adjacent vertex values.

Using the notation of [8], let $\mathcal{C}_{\mathcal{N}}$ denote a set of coarse nodes, typically just a set of a few vertices, for a nodal equivalence class $\mathcal{N}$, e.g., of the nodes of a subdomain edge or face. We recall that an equivalence class is the ancestor of any other class which contains a subset of its set of subdomains and that a coarse node does not have any ancestors.

Let u_Ψ denote a vector of vertex values. We introduce the coarse interpolant $u_{c0} = \Psi u_\Psi$ between vertex values and nodal equivalence class averages such that each of these averages equals the average of its ancestor vertex values. Thus, a row of Ψ associated with an edge of the center subdomain in the motivating example has two entries of $1/2$ (one entry for each vertex at its ends), while all other entries are 0. We note that the number of rows in Ψ equals that of the active coarse degrees of freedom for the original BDDC preconditioner. Thus, if only edges averages are used this number equals the total number of subdomain edges.

The reduced coarse matrix is defined as $K_{cr} := \Psi^T K_c \Psi$. The number of rows and columns in K_{cr} equals the number of vertices for scalar problems. We consider the following preconditioner for K_c:

$$M_c^{-1} = \Psi K_{cr}^{-1} \Psi^T + \mathrm{diag}(K_c)^{-1}, \tag{3.6}$$

where diag denotes the diagonal of the matrix; for elasticity problems the second term on the right hand side of (3.6) is block diagonal. We note that M_c^{-1} is simply a point-wise Jacobi preconditioner with an additive coarse correction. Thus, since the number of subdomains incident to an edge (or face) is bounded, a uniform upper bound on β_2 for M_c^{-1} can be obtained using a standard coloring argument. Therefore, we will focus in the next sections on obtaining lower bound estimates for β_1. We note that higher quality local preconditioning could be designed, e.g., by replacing Jacobi smoothing by symmetric Gauss-Seidel; our theory extends directly to that case, cf. [28, Section 2.3]. We will explore such options in §7.

3.1. Auxiliary Results. We first consider the case when the originating BDDC coarse space is based on edge averages. Let H_i denote the diameter of Ω_i and h_i the diameter of its smallest element. Throughout C refers to a generic constant which is independent of H_i, h_i, and ρ_i. The following lemmas concerning averages over subdomain edges play important roles in the analysis.

LEMMA 1. *Let $\bar{u}_i$ and $\bar{u}_\mathcal{E}$ denote the averages of a finite element function u_i over Ω_i and an edge $\mathcal{E}$ of Ω_i, respectively. It holds that*

$$H_i |\bar{u}_\mathcal{E} - \bar{u}_i|^2 \leq C(1 + \log(H_i/h_i)) |u_i|^2_{H^1(\Omega_i)}.$$

Proof. The lemma follows by rewriting $\bar{u}_\mathcal{E} - \bar{u}_i = (\bar{u}_\mathcal{E} - u_i) + (u_i - \bar{u}_i)$, using the Poincaré and triangle inequalities, and [8, Lemma 3]. We note that this edge lemma holds for edges of Lipschitz regions. ∎

Let K_i denote the stiffness matrix for Ω_i and Φ_i the matrix representation of the original coarse basis functions for Ω_i. We note that each column of Φ_i is associated with one of the edges of Ω_i, and that the coarse subdomain matrix is defined by $K_{ic} := \Phi_i^T K_i \Phi_i$. Reusing the symbol u_i to also denote a vector of nodal values for Ω_i, we recall that $u_i = \Phi_i u_{ic}$ minimizes the energy $u_i^T K_i u_i$ subject to the constraints that the edge averages equal those specified in u_{ic}. Based on this connection and the equality $\rho_i |u_i|^2_{H^1(\Omega_i)} = u_i^T K_i u_i = u_{ic}^T K_{ic} u_{ic}$, we obtain the following estimate from Lemma 1.

COROLLARY 1. *It holds that*

$$\rho_i H_i |\bar{u}_\mathcal{E} - \bar{u}_i|^2 \leq C(1 + \log(H_i/h_i)) u_{ic}^T K_{ic} u_{ic}.$$

From Lemma 4.2 of [30], we obtain

LEMMA 2. *Let $\mathcal{S}_{i\mathcal{E}}$ denote the set of subdomain edges of Ω_i. If $|\mathcal{S}_{i\mathcal{E}}| < C$, it holds that*

$$(1 + \log(H_i/h_i)) u_{ic}^T K_{ic} u_{ic} \leq C \rho_i H_i \max_{\mathcal{E} \in \mathcal{S}_{i\mathcal{E}}} |\bar{u}_\mathcal{E}|^2.$$

REMARK 1. *The proof of Lemma 4.2 of [30] assumes that Ω_i is a shape-regular polyhedron. If a similar lemma could be proven for general Lipschitz Ω_i, then our estimate for β_1 would also hold for Lipschitz subdomains. As for the assumptions needed for proving the basic estimates for BDDC and FETI–DP, we note that inequalities for subdomain edges and faces are central, see [28, Section 4.6] in which technical tools for polyhedral subdomains are developed. For extensions to Lipschitz subdomains, see [3, Lemma 4.7] and [8, Lemma 3]. We also note that theory has been developed for less regular subdomains for problems in the plane; see, e.g., [18].*

We next consider the case where the originating BDDC coarse space is based on face averages and start by a counterpart of Lemma 1 for subdomain faces.

LEMMA 3. *Let $\bar{u}_{\mathcal{F}}$ denote the average of a finite element function u_i over a face $\mathcal{F}$ of Ω_i. It holds that*

$$H_i|\bar{u}_{\mathcal{F}} - \bar{u}_i|^2 \leq C|u_i|^2_{H^1(\Omega_i)}.$$

Proof. It follows from a trace theorem [1, Theorem 1.6.6] and Poincaré's inequality that

$$\|u_i - \bar{u}_i\|^2_{L^2(\mathcal{F})} \leq CH_i|u_i|^2_{H^1(\Omega_i)}.$$

This estimate together with the Cauchy-Schwarz inequality gives

$$\begin{aligned}|\mathcal{F}||\bar{u}_{\mathcal{F}} - \bar{u}_i| = |\int_{\mathcal{F}} (u_i - \bar{u}_i)\,dx| \leq \int_{\mathcal{F}} |u_i - \bar{u}_i|\,dx \leq |\mathcal{F}|^{1/2}\|u_i - \bar{u}_i\|_{L^2(\mathcal{F})} \\ \leq C|\mathcal{F}|^{1/2}H_i|u_i|_{H^1(\Omega_i)}.\end{aligned}$$

The lemma then follows provided that $H_i^2/|\mathcal{F}|$ is bounded. ∎

The following corollary is obtained from Lemma 3 and $\rho_i|u_i|^2_{H^1(\Omega_i)} = u_{ic}^T K_{ic} u_{ic}$ for $u_i = \Phi_i u_{ic}$.

COROLLARY 2. *It holds that*

$$\rho_i H_i|\bar{u}_{\mathcal{F}} - \bar{u}_i|^2 \leq C u_{ic}^T K_{ic} u_{ic}.$$

The counterpart of Lemma 2 for subdomain faces is given by the following lemma.

LEMMA 4. *Let $\mathcal{S}_{i\mathcal{F}}$ denote the set of subdomain faces for Ω_i. It holds for a shape-regular polyhedron that*

$$u_{ic}^T K_{ic} u_{ic} \leq C\rho_i H_i \max_{\mathcal{F}\in\mathcal{S}_{i\mathcal{F}}} |\bar{u}_{\mathcal{F}} - \bar{u}_i|^2,$$

where the vector u_{ic} contains the averages of u_i over these faces.

Proof. The basic idea is to construct approximate coarse basis functions and establish estimates for them. These estimates will then also hold for the actual coarse basis functions because of their energy minimizing properties.

Consider a cubic subdomain of length H in each of the three coordinate directions. A coarse mesh of this subdomain has 8 smaller hexahedral elements which are also cubic in shape and 27 nodes. Let $\hat{K}_i$ denote the assembled stiffness matrix for these 8 elements and $\hat{\Phi}$ the matrix representation of the associated face basis functions. The basis function which minimizes energy subject to a unit average on the right face and zero averages for the other five faces is shown in Figure 3.1. The matrix $\hat{\Phi}$ with faces ordered left, right, front, back, bottom, top is given by

$$\hat{\Phi}^T = (1/6)\begin{bmatrix}
4 & -3 & -2 & 6 & -1 & 0 & 4 & -3 & -2 & 6 & -1 & 0 & 8 & 1 & 2 & 6 & -1 & 0 & 4 & -3 & -2 & 6 & -1 & 0 & 4 & -3 & -2 \\
-2 & -3 & 4 & 0 & -1 & 6 & -2 & -3 & 4 & 0 & -1 & 6 & 2 & 1 & 8 & 0 & -1 & 6 & -2 & -3 & 4 & 0 & -1 & 6 & -2 & -3 & 4 \\
4 & 6 & 4 & -3 & -1 & -3 & -2 & 0 & -2 & 6 & 8 & 6 & -1 & 1 & -1 & 0 & 2 & 0 & 4 & 6 & 4 & -3 & -1 & -3 & -2 & 0 & -2 \\
-2 & 0 & -2 & -3 & -1 & -3 & 4 & 6 & 4 & 0 & 2 & 0 & -1 & 1 & -1 & 6 & 8 & 6 & -2 & 0 & -2 & -3 & -1 & -3 & 4 & 6 & 4 \\
4 & 6 & 4 & 6 & 8 & 6 & 4 & 6 & 4 & -3 & -1 & -3 & -1 & 1 & -1 & -3 & -1 & -3 & -2 & 0 & -2 & 0 & 2 & 0 & -2 & 0 & -2 \\
-2 & 0 & -2 & 0 & 2 & 0 & -2 & 0 & -2 & -3 & -1 & -3 & -1 & 1 & -1 & -3 & -1 & -3 & 4 & 6 & 4 & 6 & 8 & 6 & 4 & 6 & 4
\end{bmatrix},$$

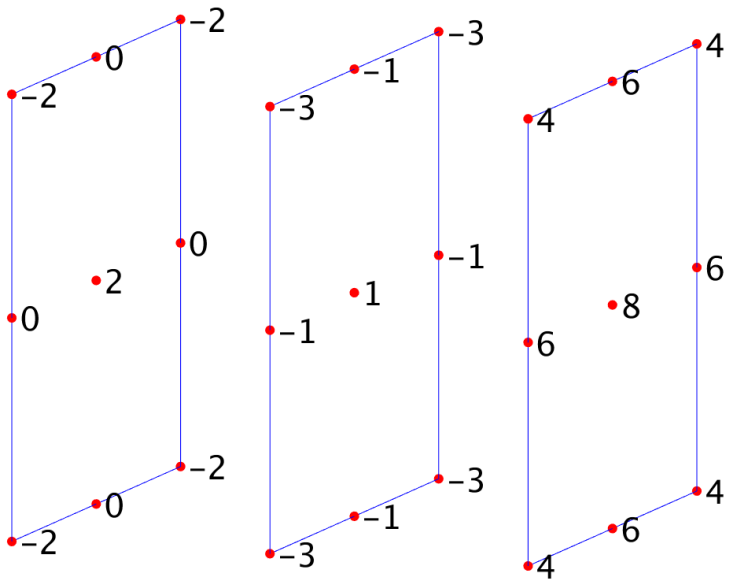

FIG. 3.1. *Approximate coarse basis function for right face of cube. Coarse basis function values shown adjacent to nodes have been multiplied by 6.*

where nodes are numbered consecutively from left to right, then front to back, and then bottom to top. One can verify that the stiffness matrix $\hat{K}_{ic} := \hat{\Phi}^T \hat{K}_i \hat{\Phi}$ associated with this coarse discretization is given by

$$\hat{K}_{ic} = \rho_i H/3 \begin{bmatrix} 11 & 5 & -4 & -4 & -4 & -4 \\ 5 & 11 & -4 & -4 & -4 & -4 \\ -4 & -4 & 11 & 5 & -4 & -4 \\ -4 & -4 & 5 & 11 & -4 & -4 \\ -4 & -4 & -4 & -4 & 11 & 5 \\ -4 & -4 & -4 & -4 & 5 & 11 \end{bmatrix}.$$

One can also verify that $x^T \hat{K}_{ic} x \leq x^T B_{ic} x$ for all 6-vectors x, where

$$B_{ic} := 4\rho_i H/3 \begin{bmatrix} 5 & -1 & -1 & -1 & -1 & -1 \\ -1 & 5 & -1 & -1 & -1 & -1 \\ -1 & -1 & 5 & -1 & -1 & -1 \\ -1 & -1 & -1 & 5 & -1 & -1 \\ -1 & -1 & -1 & -1 & 5 & -1 \\ -1 & -1 & -1 & -1 & -1 & 5 \end{bmatrix}.$$

From $x^T B_{ic} x = 4\rho_i H/3 \sum_{i,j=1}^{6} |x_i - x_j|^2$, writing $\bar{u}_{\mathcal{F}_k} - \bar{u}_{\mathcal{F}_m} = (\bar{u}_{\mathcal{F}_k} - \bar{u}_i) + (\bar{u}_i - \bar{u}_{\mathcal{F}_m})$, and using the triangle inequality, we then find

$$u_{ic}^T \hat{K}_{ic} u_{ic} \leq C\rho_i H \sum_{k,m \in \hat{\mathcal{S}}_{i\mathcal{F}}} |\bar{u}_{\mathcal{F}_k} - \bar{u}_{\mathcal{F}_m}|^2 \leq C\rho_i H \max_{\mathcal{F} \in \mathcal{S}_{i\mathcal{F}}} |\bar{u}_{\mathcal{F}} - \bar{u}_i|^2,$$

where $\mathcal{S}_{i\mathcal{F}}$ is the index set of subdomain faces for Ω_i. The lemma then follows since $u_{ic}^T K_{ic} u_{ic} \leq u_{ic} \hat{K}_{ic} u_{ic}$. Although the proof was done for a cubic subdomain, similar arguments can made for other shape-regular polyhedra. □

The theory for Schwarz methods (see, e.g., chapter 2 of [28]), makes use of space decompositions of the form

$$V = R_0^T V_0 + \sum_{k=1}^{M} R_k^T V_k,$$

where the first term involves the coarse space and the second term local spaces. In the context of our preconditioner for K_c, this decomposition can be written as

$$u_c = \Psi u_\Psi + \sum_{m=1}^{M} w_m e_m, \tag{3.7}$$

where Ψ is the interpolation matrix, u_Ψ is a vector of coarse node values, M is the number of edges or faces of the BDDC coarse space, and e_m is the unit vector in a coordinate direction. The scalar w_m is associated with edge or face number m. In order to obtain a lower bound for β_1 in (3.2), we need to find a u_Ψ and w_m in (3.7) such that

$$u_{c0}^T K_c u_{c0} + \sum_{m=1}^{M} w_m^2 e_m^T K_c e_m \leq C_0^2 u_c^T K_c u_c \tag{3.8}$$

where $u_{c0} := \Psi u_\Psi$ and C_0^2 is a constant. It then holds that $\beta_1 \geq 1/C_0^2$, see [28, Lemma 2.5]. We note that that $e_m^T K_c e_m$ is simply the diagonal entry in row m of K_c. Our strategy will be to first obtain estimates for $(u_c - u_{c0})^T K_c (u_c - u_{c0})$ and then estimates for the sum of the local contributions in (3.8). An upper bound for β_2 will be given in §4.3.

4. Analysis of the Scalar Case. The following assumption is almost identical to Assumptions 4.5 of [8] and is needed for the analysis when the originating BDDC coarse space is based on edges. For early work using similar assumptions in the study of multi-level Schwarz algorithms, see [9].

ASSUMPTION 1. *Let c be any coarse node (vertex) of Ω_i and $\mathcal{S}_c$ be the index set of all subdomains containing c on their boundaries. Select $j_c \in \mathcal{S}_c$ such that $\rho_{j_c} \geq \rho_j$ for all $j \in \mathcal{S}_c$. Assume there exists a constant C and for any $i \in \mathcal{S}_c$ a sequence $\{i = j_c^0, j_c^1, \ldots, j_c^p = j_c\}$, all in $\mathcal{S}_c$, such that $\rho_i \leq C\rho_{j_c^\ell}$ and that $\Omega_{j_c^{\ell-1}}$ and $\Omega_{j_c^\ell}$ have a subdomain edge in common for all $\ell = 1, \ldots, p$ and $i = 1, \ldots, N$.*

Assumption 1 basically says that there is an edge-connected path between Ω_i and Ω_{j_c} such that the diffusion coefficient ρ_i is no greater than a constant times the diffusion coefficient of any subdomain along the path. If Assumption 1 is satisfied, then we say there are *quasi-monotone edge-connected paths*.

The analysis of face-based coarse spaces requires a stronger condition than in Assumption 1.

ASSUMPTION 2. *Let c be any coarse node (vertex) of Ω_i and $\mathcal{S}_c$ be the index set of all subdomains containing c on their boundaries. Select $j_c \in \mathcal{S}_c$ such that $\rho_{j_c} \geq \rho_j$ for all $j \in \mathcal{S}_c$. Assume there exists a constant C and for any $i \in \mathcal{S}_c$ a sequence $\{i = j_c^0, j_c^1, \ldots, j_c^p = j_c\}$, all in $\mathcal{S}_c$, such that $\rho_i \leq C\rho_{j_c^\ell}$ and that $\Omega_{j_c^{\ell-1}}$ and $\Omega_{j_c^\ell}$ have a subdomain face in common for all $\ell = 1, \ldots, p$ and $i = 1, \ldots, N$.*

Assumption 2 basically says that there is a face-connected path between Ω_i and Ω_{j_c} such that the diffusion coefficient ρ_i is no greater than a constant times the diffusion coefficient of any subdomain along the path. If Assumption 2 is satisfied, then we say there are *quasi-monotone face-connected paths*.

The next assumption basically says that the ratio H_m/h_m does not vary too much for any subdomain Ω_m containing c.

ASSUMPTION 3. *Let $\mathcal{S}_c$ be as defined in Assumption 1. It is assumed for any coarse node c that*

$$\max_{j,k\in\mathcal{S}_c}(H_j/h_j)/(H_k/h_k) < C.$$

4.1. Analysis of the Coarse Components. The present goal is to construct a coarse interpolant $u_{c0} = \Psi u_\Psi$ between coarse node values and equivalence class averages, and then to obtain estimates for $u_{c0}^T K_c u_{c0}$ in terms of $u_c^T K_c u_c$. We first consider the case when the original BDDC coarse space is based on subdomain edge averages.

4.1.1. Edge-Based Coarse Space. The value at coarse node c is chosen as $\bar{u}_{j_c}$, where j_c is defined in Assumption 1. If the interpolation of an edge $\mathcal{E}$ of Ω_i only involves a single coarse node c, i.e. the row of Ψ associated with this edge has a single nonzero value of 1 in the column for c, then the coarse approximation of $\bar{u}_\mathcal{E}$ is given by $\bar{u}_{\mathcal{E}0} = \bar{u}_{j_c}$.

To simplify the notation in the following development, we replace $\{i, j_c^1, \ldots, j_c^p\}$ in Assumption 1 by $\{0, 1, \ldots, p\}$ and label the edges of the connected path between Ω_i and $\Omega_{j_c^p}$ as $\mathcal{E}_1, \ldots, \mathcal{E}_p$. We note that with this convention that $\Omega_{\ell-1}$ and Ω_ℓ share edge $\mathcal{E}_\ell$ for $\ell = 1, \ldots, p$, and that the edges $\mathcal{E}_\ell$ and $\mathcal{E}_{\ell+1}$ both belong to subdomain Ω_ℓ for $\ell = 1, \ldots, p-1$. We have

$$\bar{u}_\mathcal{E} - \bar{u}_{\mathcal{E}0} = (\bar{u}_\mathcal{E} - \bar{u}_{\mathcal{E}_1}) + \sum_{\ell=1}^{p-1}((\bar{u}_{\mathcal{E}_\ell} - \bar{u}_\ell) + (\bar{u}_\ell - \bar{u}_{\mathcal{E}_{\ell+1}})) + (\bar{u}_{\mathcal{E}_p} - \bar{u}_{j_c}). \tag{4.1}$$

Since the edge averages for each term in parenthesis involve the same subdomain, it follows from Corollary 1 and Assumption 1 that

$$\rho_i H_i |\bar{u}_\mathcal{E} - \bar{u}_{\mathcal{E}0}|^2 \leq C \sum_{j\in\mathcal{S}_c}(1 + \log(H_j/h_j)) u_{jc}^T K_{jc} u_{jc}. \tag{4.2}$$

We note that (4.2) also holds if $\bar{u}_{\mathcal{E}0}$ depends on two coarse nodes c_1 and c_2 rather than just a single one. To see this, we note that

$$\bar{u}_\mathcal{E} - \bar{u}_{\mathcal{E}0} = \bar{u}_\mathcal{E} - (\bar{u}_{j_{c_1}} + \bar{u}_{j_{c_2}})/2 = (\bar{u}_\mathcal{E} - \bar{u}_{j_{c_1}})/2 + (\bar{u}_\mathcal{E} - \bar{u}_{j_{c_2}})/2,$$

and that (4.2) can then be used for each of the terms on the right hand side.

It follows from (4.2) and Lemma 2 that

$$(u_{ic} - u_{ic0})^T K_{ic}(u_{ic} - u_{ic0}) \leq C \sum_{j\in\mathcal{M}_i} u_{jc}^T K_{jc} u_{jc},$$

where $u_{ic0} = R_{ic} u_{c0}$ is the coarse interpolant of u_{ic} and $\mathcal{M}_i$ is the index set of all subdomains adjacent to Ω_i and also including Ω_i. Assumption 3 was used to allow for a cancellation of the $1 + \log(H_j/h_j)$ factors. Summing this estimate over all subdomains and noting that $|\mathcal{M}_i| \leq C$, we find

$$(u_c - u_{c0})^T K_c (u_c - u_{c0}) \leq C u_c K_c u_c. \tag{4.3}$$

4.1.2. Face-Based Coarse Space. A similar analysis can be carried out for a face-based BDDC coarse space by replacing Corollary 1 and Lemma 2 by Corollary 2 and Lemma 4, respectively. Further, Assumption 2 is used and the telescoping sum in (4.1) now involves face averages rather than edge averages. Logarithmic factors no longer enter into the analysis, and we again arrive at an estimate as in (4.3).

4.2. Local Analysis. Let $w := u_c - u_{c0}$. We find from (4.2) that, for the edge-based case,

$$\rho_i H_i w_m^2 \leq C \sum_{j \in \mathcal{S}_c} (1 + \log(H_j/h_j)) u_{jc}^T K_{jc} u_{jc},$$

where m is the row of Ψ corresponding to edge $\mathcal{E}$ of Ω_i. Setting the row of u_{ic} in Lemma 2 corresponding to $\mathcal{E}$ to 1 and all other rows to zero gives

$$(1 + \log(H_i/h_i)) k_{icmm} \leq C \rho_i H_i,$$

where k_{icmm} is the diagonal entry of K_{ic} corresponding to $\mathcal{E}$. Let $\mathcal{M}_\mathcal{E}$ denote the index set of subdomains containing $\mathcal{E}$ and define $\hat{\mathcal{M}}_\mathcal{E} := \cup_{i \in \mathcal{M}_\mathcal{E}} \mathcal{M}_i$. From the previous two estimates and Assumption 3, we obtain

$$w_m^2 e_m^T K_c e_m = w_m^2 \sum_{j \in \mathcal{M}_\mathcal{E}} k_{jcmm} \leq C \sum_{j \in \hat{\mathcal{M}}_\mathcal{E}} u_{jc}^T K_{jc} u_{jc}.$$

Summing this estimate over all edges and noting that the number of elements of $\hat{\mathcal{M}}_\mathcal{E}$ containing the index j is bounded by a constant, we find that

$$\sum_{m=1}^{M} w_m^2 e_m^T K_c e_m \leq C u_c^T K_c u_c. \tag{4.4}$$

We note that (4.4) also holds for a face-based coarse space under Assumption 2 by using a similar analysis involving Lemma 4 rather than Lemma 2.

4.3. Two Main Results. We are now ready to provide results for scalar elliptic problems for edge- and face-based BDDC algorithms.

THEOREM 1. *For edge-based BDDC coarse spaces and with quasi-monotone edge-connected paths (see Assumption 1), the condition number of the preconditioned operator that is obtained by replacing the direct solver for the coarse problem by the preconditioner M_c^{-1} defined in (3.6) is bounded by*

$$\kappa_a \leq C(1 + \log(H/h))^2.$$

Proof. With reference to (3.5), it follows from a coloring argument that $\max(1, \beta_2) \leq C$ since each subdomain edge is common to a finite number of subdomains. From the estimate in (4.3) and the triangle inequality, we find

$$u_{c0}^T K_c u_{c0} \leq C u_c^T K_c u_c.$$

Together with the local estimate in (4.4), it follows that (3.8) holds with

$$C_0^2 \leq C,$$

and thus

$$\frac{\max(1, \beta_2)}{\min(1, \beta_1)} \leq C.$$

The theorem then follows from (3.5) since κ is bounded by $C(1 + \log(H/h))^2$ for edge-based coarse spaces under Assumption 1 (cf. Algorithm D in [28, Section 6.4.2]). ∎

THEOREM 2. *For face-based BDDC coarse spaces and with quasi-monotone face-connected paths (see Assumption 2), the condition number of the preconditioned operator that is obtained by replacing the direct solver for the coarse problem by the preconditioner M_c^{-1} defined in (3.6) is bounded by*

$$\kappa_a \leq C(1+\log(H/h))^2.$$

An additional factor of $1+\log(H/h)$ appears in this estimate under the weaker Assumption 1.

Proof. This estimate is obtained in the same way as for Theorem 1, but using estimates for faces rather than edges. The additional factor of $1+\log(H/h)$ appears for the weaker Assumption 1 because there is no longer a cancellation of a logarithmic factor when using Lemma 4 for faces rather than Lemma 2 for edges. In addition, the estimate $\kappa \leq C(1+\log(H/h))^2$ for a face-based coarse space can be found in Theorem 6 of [23]. See also [20]. □

5. Compressible Linear Elasticity. We now turn to the equations of linear elasticity: Let $\Omega \subset \boldsymbol{R}^3$ be a domain with a Lipschitz boundary, and let $\partial\Omega_D$ be a nonempty subset, of positive measure, of its boundary $\partial\Omega$, and introduce the Sobolev space $\mathbf{V} := \{\mathbf{v} \in \mathbf{H}^1(\Omega) : \mathbf{v}|_{\partial\Omega_D} = 0\}$. Here, $\mathbf{H}^1(\Omega) := H^1(\Omega)^3$. The linear elasticity problem consists in finding the displacement $\mathbf{u} \in \mathbf{V}$ of the domain Ω, fixed along $\partial\Omega_D$ and subject to a surface force of density $\mathbf{g}$, along $\partial\Omega_N := \partial\Omega \setminus \partial\Omega_D$, and a body force $\mathbf{f}$:

$$a(\mathbf{u},\mathbf{v}) := 2\int_\Omega \mu\ \epsilon(\mathbf{u}) : \epsilon(\mathbf{v})\ dx + \int_\Omega \lambda\ \text{div}\ \boldsymbol{u}\ \text{div}\ \boldsymbol{v}\ dx\ =\ \langle \mathbf{F},\mathbf{v}\rangle \quad \forall \mathbf{v} \in \mathbf{V}.$$

Here $\lambda(x)$ and $\mu(x)$ are the Lamé parameters, $\epsilon_{ij}(\mathbf{u}) = \frac{1}{2}(\frac{\partial u_i}{\partial x_j} + \frac{\partial u_j}{\partial x_i})$ is the linearized strain tensor, and two inner products are defined by

$$\epsilon(\mathbf{u}) : \epsilon(\mathbf{v}) := \sum_{i=1}^3 \sum_{j=1}^3 \epsilon_{ij}(\mathbf{u})\epsilon_{ij}(\mathbf{v}),\ \langle \mathbf{F},\mathbf{v}\rangle\ :=\ \int_\Omega \sum_{i=1}^3 f_i v_i\ dx + \int_{\partial\Omega_N} \sum_{i=1}^3 g_i v_i\ ds. \tag{5.1}$$

The Lamé parameters can be expressed in terms of the Poisson ratio ν and Young's modulus E:

$$\mu = \frac{E}{2(1+\nu)}, \qquad \lambda = \frac{E\nu}{(1+\nu)(1-2\nu)} = \frac{2\nu}{1-2\nu}\mu.$$

In our proofs, we will always assume that the Lamé parameters are constant in each subdomain and denote their values in Ω_i by μ_i and λ_i, respectively. The parameter μ_i will play a role similar to that of ρ_i in the analysis of the scalar case. When developing our theory, we will assume that this Lamé parameter satisfies Assumption 2.

5.1. Korn's Inequalities. We note that the factor $\frac{2\nu}{1-2\nu}$ is bounded for the compressible case for which $\nu < 1/2$. We can then derive the upper bound

$$a_i(\mathbf{u},\mathbf{u}) \leq \frac{2(1+\nu_i)}{1-2\nu_i}\mu_i |\mathbf{u}|^2_{\mathbf{H}^1(\Omega_i)},$$

where $a_i(\mathbf{u},\mathbf{v})$ is the contribution of Ω_i to $a(\mathbf{u},\mathbf{v})$. The ellipticity of this problem is established by using a Korn inequality; for a discussion of the Korn inequalities, see [4, Section 6.15]. In particular, we will use [4, Theorem 6.15-1]: there exists a constant $C = C(\Omega_i)$, invariant under dilation, such that,

$$|\boldsymbol{u}|^2_{\mathbf{H}^1(\Omega_i)} + (1/H_i^2)\|\boldsymbol{u}\|^2_{L^2(\Omega_i)} \leq C\big(\int_{\Omega_i} \epsilon(\boldsymbol{u}) : \epsilon(\boldsymbol{u})\ dx + (1/H_i^2)\|\boldsymbol{u}\|^2_{L^2(\Omega_i)}\big), \tag{5.2}$$

where H_i is the diameter of Ω_i. We also will use [4, Theorem 6.15-3]: there exists a constant $C = C(\Omega_i)$, invariant under dilation, such that,

$$\inf_{\boldsymbol{r}\in\mathcal{RB}} \|\boldsymbol{u}-\boldsymbol{r}\|^2_{L^2(\Omega_i)} \leq CH_i^2 \int_{\Omega_i} \epsilon(\boldsymbol{u}) : \epsilon(\boldsymbol{u})\ dx. \tag{5.3}$$

Here $\mathcal{RB}$ is the six-dimensional space of rigid body modes, the null space of the elasticity operator. This second estimate will, essentially, replace Poincaré's inequality.

Given the Korn inequalities and the $\mathbf{H}^1-$continuity of the bilinear form $a_i(\mathbf{u},\mathbf{v})$, we can use the $\mathbf{H}^1(\Omega)-$norm in most of our analysis.

5.2. Analysis for Linear Elasticity. Looking back at the scalar case and formula (4.1) and the proof of (4.2), we find a need to replace the edge and subdomain averages by expressions appropriate for elasticity. We note that (4.1) provides a sum of differences of pairs of terms associated with the same subdomain, which allows us to shift by elements in the null space, i.e., by constants. This suggests that we should now try to find rigid body modes that will serve the same purpose.

We will consider the BDDC variants with the primal space defined by the averages over the three components of the displacement over all the subdomain edges and also the case defined by six primal face constraints for each subdomain face. In fact, we could also obtain the same results for variants where any subdomain face is associated with either edge or face constraints or both. By using results reported in [19], we can directly establish a bound on the condition number, in the edge case, of the preconditioned operator of the form $C(1+\log(H/h))^2$ if Assumption 2 is satisfied. Thus, if all the subdomain edges are subject to three average constraints, we can then use [19, Proposition 5.1 and Definition 5.3], to establish that all our subdomain faces are *fully primal*. Combining this observation with Assumption 2, we find that we have an *acceptable set of primal constraints*, as in [19, Definition 5.8], and that we can use the analysis of [19, Subsection 8.4] to conclude that we have a $C(1+\log(H/h))^2$ bound for the BDDC algorithm prior to the introduction of an inexact solver for the coarse component of the preconditioner. These arguments can easily be modified to cover the case with face constraints by working out an alternative representation of arbitrary rigid body modes as in [19, Section 8.4]; we replace the edge functionals, denoted by g_n below, by $L^2(\mathcal{F})-$inner products of $\boldsymbol{u}$ and the basis functions $\boldsymbol{r}_k$ of $\mathcal{RB}$ as indicated at the end of §5.2.1.

We note that a richer primal space is required, to obtain a satisfactory rate of convergence, for certain sets of Lamé parameters of the subdomains. That conclusion is supported by numerical experiments reported in [15]. The two papers, [15, 19], concern FETI–DP algorithms but BDDC and FETI–DP algorithms are closely related since the operators relevant for the convergence rates of the two have the same eigenvalues except possibly for two if the same primal space is used and the coarse problems are solved exactly, see [24]. Related issues on the effect of the values of the Lamé parameters in the subdomains are also discussed in [26], a recent paper on isogeometric analysis, which also provides experimental evidence.

5.2.1. Counterparts of (4.1), (4.2), and (4.3). We now turn to developing bounds specific to elasticity and this paper. We will borrow tools developed in [19] and will also find that our arguments will be simpler than those in that earlier study.

Let $\mathcal{E}$ be any subdomain edge of any subdomain Ω_i and let the subdomain vertex $\boldsymbol{c}$ be one of the endpoints of $\mathcal{E}$. Let $\bar{\boldsymbol{u}}_{\mathcal{E}}$ be the $3-$vector of averages over $\mathcal{E}$ of the components of $\boldsymbol{u}$. According to Assumption 2, we have a quasi-monotone face-connected path from Ω_i to a subdomain Ω_{j_p} with the largest Lamé parameter μ of the subdomains which share that subdomain vertex. As in Subsection 4.1.1, we renumber the subdomains on the path by $\{0,1,\ldots,p\}$ and denote the subdomain face between $\Omega_{\ell-1}$ and Ω_ℓ by $\mathcal{F}_\ell$. We also select an additional subdomain face $\mathcal{F}_0$ of Ω_0, which is different from $\mathcal{F}_1$ and with a boundary which contains the subdomain edge $\mathcal{E}$. Then for $0 \leq \ell \leq p-1$, the faces $\mathcal{F}_\ell$ and $\mathcal{F}_{\ell+1}$ are associated with subdomain Ω_ℓ on the path. For the final subdomain on the path, Ω_p, we will only work with one face, $\mathcal{F}_p$.

We will estimate the ℓ^2-norm of $\bar{\boldsymbol{u}}_{\mathcal{E}} - \bar{\boldsymbol{r}}_{\mathcal{E}}^{(p)}$ where $\boldsymbol{r}^{(p)} \in \mathcal{RB}$. This $\boldsymbol{r}^{(p)}$ will provide the coarse approximation of $\boldsymbol{u}$ associated with the subdomain vertex $\boldsymbol{c}$ and is independent of the edge $\mathcal{E}$. We will not work directly with this $3-$vector but instead with an element in $\mathcal{RB}$ with the three components of these vectors as coefficients for $\boldsymbol{r}_1, \boldsymbol{r}_2$, and $\boldsymbol{r}_3$, respectively. The $\boldsymbol{r}_k$ form a standard basis of $\mathcal{RB}$:

$$\boldsymbol{r}_1 := (1,0,0)^T, \boldsymbol{r}_2 := (0,1,0)^T, \boldsymbol{r}_3 := (0,0,1)^T, \boldsymbol{r}_4 := (1/H_i)(0, -x_3 + x_3^o, x_2 - x_2^o)^T,$$
$$\boldsymbol{r}_5 := (1/H_i)(x_3 - x_3^o, 0, -x_1 + x_1^o)^T, \boldsymbol{r}_6 := (1/H_i)(-x_2 + x_2^o, x_1 - x_1^o, 0)^T.$$

Here $\boldsymbol{x}^o := (x_1^o, x_2^o, x_3^o)^T$ is the origin of the coordinate system. We have scaled $\boldsymbol{r}_4, \boldsymbol{r}_5$, and $\boldsymbol{r}_6$ by dividing by H_i to make the norms of these six basis functions of the same order. We will write this element of $\mathcal{RB}$, representing $\bar{\boldsymbol{u}}_{\mathcal{E}} - \bar{\boldsymbol{r}}_{\mathcal{E}}^{(p)}$, as a sum of differences of pairs of elements in $\mathcal{RB}$ associated with the individual subdomains on the path.

We will work with functionals $g_i^{\mathcal{E},\mathcal{F}}, i = 1, 2$, and 3 and $f_k^{\mathcal{F}}, k = 1, \ldots, 6$, as introduced in [19, Section 5], which provide important tools in the proof of the main results of that paper. These functionals are associated with a particular subdomain face $\mathcal{F}$ and we will choose the origin of the coordinate system, $\boldsymbol{x}^o$, in which we express the basis of the rigid body space, as a point on or close to the face.

For the first face, $\mathcal{F}_0$, we will use the centroid of $\mathcal{E}$ as the origin of the coordinate system. Then,

$$\int_{\mathcal{E}} \boldsymbol{r}_k^{\mathcal{F}_0} ds = 0 \quad \textit{for } k = 4, 5, \textit{ and } 6. \tag{5.4}$$

We now introduce the functionals

$$g_i^{\mathcal{E}',\mathcal{F}_0}(\boldsymbol{u}^{(0)}) := \frac{\int_{\mathcal{E}'} u_i^{(0)} ds}{\int_{\mathcal{E}'} 1 ds}, i = 1, 2, \textit{ and } 3,$$

where $\mathcal{E}'$ is any subdomain edge of the face $\mathcal{F}_0$ under consideration and $u_i^{(0)}$ one of the three components of $\boldsymbol{u}^{(0)}$, the restriction of $\boldsymbol{u}$ to subdomain Ω_i. The number of such functionals equals three times the number of subdomain edges that form the boundary of the face; when discussing the edge-based case, we will assume that each face has at least three such edges. According to [19, Proposition 5.1], we can then always find six linearly independent functionals of this set. We then form a dual basis of $\mathcal{RB}$ by constructing the $f_k^{\mathcal{F}_0}$ as linear combinations of these $g_i^{\mathcal{E}',\mathcal{F}_0}$. They satisfy $f_k^{\mathcal{F}_0}(\boldsymbol{r}_\ell) = \delta_{k\ell}$ and we then have a representation of any element $\boldsymbol{r} \in \mathcal{RB}$:

$$\boldsymbol{r} = \sum_{k=1}^{6} f_k^{\mathcal{F}_0}(\boldsymbol{r}) \boldsymbol{r}_k^{\mathcal{F}_0}. \tag{5.5}$$

Similar formulas are also developed for the other faces on the path. These formulas will help us shift by elements in $\mathcal{RB}$ to prepare for the use of (5.2) and (5.3).

Using (5.4), we find that that we can use the three $g_i^{\mathcal{E},\mathcal{F}}$ for the edge $\mathcal{E}$ as $f_1^{\mathcal{F}_0}, f_2^{\mathcal{F}_0}$, and $f_3^{\mathcal{F}_0}$ and then complement this set by three additional functionals $f_4^{\mathcal{F}_0}, f_5^{\mathcal{F}_0}$, and $f_6^{\mathcal{F}_0}$, as in [19], e.g., by using a $QR-$factorization with column pivoting. We note that the three components of $\bar{\boldsymbol{u}}_{\mathcal{E}}$ are then the first three coefficients of

$$\sum_{k=1}^{6} f_k^{\mathcal{F}_0}(\boldsymbol{u}) \boldsymbol{r}_k^{\mathcal{F}_0}.$$

Given that the $\boldsymbol{r}_k^{\mathcal{F}_0}$ are linearly independent, we can then bound the components of $\bar{\boldsymbol{u}}_{\mathcal{E}}$ by the $L_2(\mathcal{E})-$norm of this function.

Bounds for the $g_i^{\mathcal{E},\mathcal{F}_\ell}$ are given in detail in [19] and involve one logarithmic factor and the $\boldsymbol{H}^1(\Omega_\ell)-$norm of $\boldsymbol{u}^{(\ell)}$. By an argument using linear independence, we can then show that we have the same bounds for the functionals $f_k^{\mathcal{F}_\ell}$. Thus, we have

$$|f_k^{\mathcal{F}_\ell}(\boldsymbol{u})|^2 \leq CH_i^{-1}(1+\log(H_i/h_i))(|\boldsymbol{u}|^2_{\boldsymbol{H}^1(\Omega_\ell)} + (1/H_i)^2\|\boldsymbol{u}\|^2_{L_2(\Omega_\ell)}).$$

When moving from Ω_0 to the next subdomain, Ω_1, we will use the fact that

$$\sum_{k=1}^{6} f_k^{\mathcal{F}_1}(\boldsymbol{u}^{(0)})\boldsymbol{r}_k^{\mathcal{F}_1} = \sum_{k=1}^{6} f_k^{\mathcal{F}_1}(\boldsymbol{u}^{(1)})\boldsymbol{r}_k^{\mathcal{F}_1}.$$

This follows from the choice of primal constraints, which ensures that all the $g_i^{\mathcal{E},\mathcal{F}_1}$ functionals associated with the subdomain edges of the face $\mathcal{F}^1$ have the same values for $\boldsymbol{u}^{(0)}$ and $\boldsymbol{u}^{(1)}$. The same argument can also be used for all other subdomain faces on the face-connected path.

Therefore, we can now write

$$\sum_{k=1}^{6} f_k^{\mathcal{F}_0}(\boldsymbol{u}^{(0)}-\boldsymbol{r}^{(p)})\boldsymbol{r}_k^{\mathcal{F}_0} = (\sum_{k=1}^{6} f_k^{\mathcal{F}_0}(\boldsymbol{u}^{(0)}-\boldsymbol{r}^{(p)})\boldsymbol{r}_k^{\mathcal{F}_0} - \sum_{k=1}^{6} f_k^{\mathcal{F}_1}(\boldsymbol{u}^{(0)}-\boldsymbol{r}^{(p)})\boldsymbol{r}_k^{\mathcal{F}_1}) + \ldots$$
$$+(\sum_{k=1}^{6} f_k^{\mathcal{F}_\ell}(\boldsymbol{u}^{(\ell)}-\boldsymbol{r}^{(p)})\boldsymbol{r}_k^{\mathcal{F}_\ell} - \sum_{k=1}^{6} f_k^{\mathcal{F}_{\ell+1}}(\boldsymbol{u}^{(\ell)}-\boldsymbol{r}^{(p)})\boldsymbol{r}_k^{\mathcal{F}_{\ell+1}}) + \ldots + \sum_{k=1}^{6} f_k^{\mathcal{F}_p}(\boldsymbol{u}^{(p)}-\boldsymbol{r}^{(p)})\boldsymbol{r}_k^{\mathcal{F}_p}.$$

The first subdomain on the path, Ω_0, contributes

$$\sum_{k=1}^{6} f_k^{\mathcal{F}_0}(\boldsymbol{u}^{(0)}-\boldsymbol{r}^{(p)})\boldsymbol{r}_k^{\mathcal{F}_0} - \sum_{k=1}^{6} f_k^{\mathcal{F}_1}(\boldsymbol{u}^{(0)}-\boldsymbol{r}^{(p)})\boldsymbol{r}_k^{\mathcal{F}_1}.$$

We can now replace $\boldsymbol{r}^{(p)}$ by $\boldsymbol{r}^{(0)}$ by using (5.5); we simply subtract and add $\boldsymbol{r}^{(0)}-\boldsymbol{r}^{(p)}$ and group the terms appropriately. Here $\boldsymbol{r}^{(0)}$ is the element of $\mathcal{RB}$ obtained in (5.3) and we have then eliminated the L_2-term. By using (5.2) as well as (5.3), we are able to return to the use of the bilinear form for the elasticity operator; up to this point, we have used the $\boldsymbol{H}^1-$norm.

The similar expressions, associated with all but the final subdomain on the path, can be handled in the same way. The fact that we only use one face of Ω_p poses no problem since we have $\boldsymbol{r}^{(p)}$ at our disposal.

We can now establish estimates that are counterparts of (4.2) and (4.3):

$$\mu_i H_i|\bar{\boldsymbol{u}}_{\mathcal{E}} - \bar{\boldsymbol{r}}_{\mathcal{E}}^{(p)}|^2 \leq C\sum_{j\in\mathcal{S}_c}(1+\log(H_j/h_j))\boldsymbol{u}_{jc}^T K_{jc}\boldsymbol{u}_{jc}. \tag{5.6}$$

and by using Lemma 2,

$$(\boldsymbol{u}_c-\boldsymbol{u}_{c0})^T K_c(\boldsymbol{u}_c-\boldsymbol{u}_{c0}) \leq C\boldsymbol{u}_c K_c\boldsymbol{u}_c. \tag{5.7}$$

For the case based on face constraints, we can replace the $g_i^{\mathcal{E},\mathcal{F}}$ functionals by

$$g_k^{\mathcal{F}}(\boldsymbol{u}) := \frac{\int_{\mathcal{F}} \boldsymbol{u}\cdot\boldsymbol{r}_k dA}{\int_{\mathcal{F}} \boldsymbol{r}_k\cdot\boldsymbol{r}_k dA},\ k=1,\ldots,6.$$

There are now only six functionals and we can easily introduce a basis for the dual space, i.e., $f_k^{\mathcal{F}}$ functionals that can be used as in the edge-based case. This is in fact an easier case.

5.2.2. Local Analysis. The analysis closely follows the one for the scalar case, but now $\boldsymbol{w}_m$ refers to a 3-vector of edge average displacements in the edge-based case. Defining $\boldsymbol{w} := \boldsymbol{u}_c - \boldsymbol{u}_{c0}$, it follows that

$$\mu_i H_i |\boldsymbol{w}_m|^2 \leq C \sum_{j \in \mathcal{S}_c} (1 + \log(H_j/h_j)) \boldsymbol{u}_{jc}^T K_{jc} \boldsymbol{u}_{jc},$$

where $\boldsymbol{w}_m = R_m \boldsymbol{w}$ are the three rows of $\boldsymbol{w}$ associated with edge $\mathcal{E}$ of Ω_i. Using arguments similar to those for the scalar case, we find that

$$\sum_{m=1}^{M} \boldsymbol{w}_m^T R_m K_c R_m^T \boldsymbol{w}_m \leq C \boldsymbol{u}_c^T K_c \boldsymbol{u}_c. \tag{5.8}$$

We note that $R_m K_c R_m^T$ are 3x3 matrices for all subdomain edges.

The face-based case requires no additional ideas.

5.2.3. Main Result for Elasticity. Using the same arguments as for the scalar case, we obtain the following result from the coarse and local estimates in (5.7) and (5.8).

THEOREM 3. *For edge-based and face-based BDDC coarse spaces and with quasi-monotone face-connected paths (see Assumption 2), the condition number of the preconditioned operator that is obtained by replacing the direct solver for the coarse problem by the preconditioner M_c^{-1} defined in (3.6) is bounded by*

$$\kappa_a \leq C(1 + \log(H/h))^2.$$

6. Implementation. We note that edge-based coarse spaces can sometimes be more problematic for linear elasticity than for the scalar case. For example, consider the simple case of four subdomains sharing a single edge and with a Dirichlet boundary condition applied to one of the subdomain faces. We note that the nodes on that edge are the only ones which are shared by more than two subdomain boundaries. For scalar problems this presents no difficulties since a single edge constraint is sufficient to ensure nonsingularity of the coarse and local Neumann problems. For elasticity, however, constraints on the three components of the edge average displacement are not sufficient for this purpose. One way to deal with this situation is to also include 6 constraints for each of the 4 pairs of subdomains sharing a face, but we then no longer have a purely edge-based coarse space.

Our implementation in Trilinos [12] automatically augments the original edge-based constraints with face-based ones to address problems like the one described in the previous paragraph. For example, if a subdomain face has fewer than two subdomain edges in its closure, then 6 additional face-based constraints are included for elasticity problems to restrain rigid body displacements between the two subdomains sharing the face. If the face has two edges in its closure, only 3 additional constraints associated with mean face displacements are needed. Finally, no additional constraints are needed if there are at least 3 edges in the closure of the face. As noted earlier, the situation is much simpler for scalar problems where only a single edge constraint is needed to constrain two adjacent subdomains.

The situation for linear elasticity is often simpler when using a face-based rather than edge-based coarse space. For example, if 3 translational and 3 rotational degrees of freedom are used, then no adjustments are needed for the four subdomain case described previously. Moreover, there are no difficulties even when the four subdomains are in a single row with only face connections between them. One downside of a face-based approach is that the coarse space can often be larger than that for an edge-based approach. The reason is that 6 constraints are used for each face compared to

3 constraints for each edge. With the present approach, however, the number of coarse degrees of freedom for each vertex is the same for either edge-based or face-based coarse spaces.

In the next section, we will explore an *economic* approach for linear elasticity in which the number of degrees of freedom for some subdomain vertices can be reduced from 6 to 3. This approach is more naturally suited to face-based coarse spaces, but can also be useful for edge-based ones in certain cases. For example, the average displacement for a straight edge can be interpolated using the average of its two bounding vertices. Similarly, if a face has 3 or more vertices in its closure which are not on the same line, then a least squares fit of the vertex displacements can be used for the interpolation of the average displacement and rotation of the face. Numerical examples in the next section demonstrate that significant reductions in coarse space dimensions are possible using this economic approach.

Our theory was developed for an additive Schwarz approach, but it can be easily adapted to a multiplicative approach (cf. Chapter 2 of [28]) like the one used in our implementation. We only discuss details for the scalar case, but they carry over in a straightforward manner for elasticity. Given a coarse residual vector r_c, the preconditioned residual $\hat{M}_c^{-1} r_c$ obtained using a multiplicative approach can be obtained as follows.

1. Calculate z_{c1} using forward Gauss-Seidel with r_c as input.
2. Calculate $r_{c1} = r_c - K_c z_{c1}$, the coarse correction $z_{c2} = \Psi K_{cr}^{-1} \Psi^T r_{c1}$, and the updated residual $r_{c2} = r_{c1} - K_c z_{c2}$.
3. Calculate z_{c3} using reverse Gauss-Seidel with r_{c2} as input.
4. Calculate $\hat{M}_c^{-1} r_c = z_{c1} + z_{c2} + z_{c3}$.

Compared to the additive preconditioner M_c in (3.6), $\hat{M}_c$ requires additional matrix-vector products involving the coarse matrix K_c, but these costs are typically much smaller than those for calculating the coarse correction $\Psi K_{cr}^{-1} \Psi^T r_c$ which is common to both preconditioners. We note that the action of $\hat{M}_c^{-1}$ is similar to applying a two-level multigrid V-cycle with symmetric Gauss-Seidel smoothing.

Our implementation allows for multiple subdomains per MPI rank. With this feature, different threads can be assigned to the work for each subdomain. In addition, this feature allows us to explore the performance of the proposed approach at very large subdomain counts without the need for the resources of a large supercomputer. Another feature of the implementation is the option of using inexact solvers (i.e. preconditioners) for the subdomain and coarse problems [7]. Although we do not present numerical results for this option, it does allow for much larger subdomains than could be reasonably accommodated by sparse direct solvers. Further, inexact solvers may play a larger role in the future because of performance challenges of sparse direct solvers on GPUs.

In certain cases, a mesh partitioner, such as METIS [14], may generate subdomains which have disconnected components. We identify these components and treat each one as its own subdomain. For unusual cases where a subdomain does not have any faces, we activate all equivalence classes associated with that subdomain. The same adjustments are made for elasticity problems if there is not at least one face with three or more nodes.

7. Numerical Results. Returning to §2, we find that the results in Tables 2.1 and 2.2 are in good agreement with the theory for the scalar case, and demonstrate that comparable performance to the standard edge-based BDDC preconditioner can be obtained more efficiently. We note that in Table 2.2 that the coarse space dimension n_c is approximately 3 times smaller for the proposed approach than that of the standard edge-based approach for larger numbers of subdomains. This can lead to large reductions in setup times since the number of operations to factor the coarse matrix scales by n_c^2.

Similar results for an elastic cube with $E = 1$ and $\nu = 0.3$ are shown in Tables 7.1-7.3 for both edge-based and face-based coarse spaces. Here again we see good agreement with theory and comparable convergence rates for the standard and proposed approaches. The coarse space dimensions are again smaller, but the reduction is more modest for elasticity and edge-based coarse

TABLE 7.1
Elasticity results. Number of iterations (iter) and condition number estimates (cond) are shown for a unit cube domain constrained on one face and decomposed into 27 smaller cubic subdomains.

	edge-based coarse space				face-based coarse space			
	standard approach		proposed approach		standard approach		proposed approach	
H/h	iter	cond	iter	cond	iter	cond	iter	cond
4	18	3.83	20	4.26	19	4.10	20	4.51
8	25	6.43	27	7.02	19	4.43	26	7.31
12	28	8.43	31	9.16	22	5.44	31	9.71
16	31	10.0	34	10.9	24	6.27	34	11.6

TABLE 7.2
Elasticity results for edge-based coarse spaces. Coarse space dimension n_c and convergence results are shown for increasing numbers of subdomains N and fixed $H/h = 8$.

	edge-based coarse spaces					
	standard approach			proposed approach		
N	n_c	iter	cond	n_c	iter	cond
64	432	26	6.76	162	28	7.14
216	1530	27	6.90	750	29	7.47
512	3780	28	6.95	2058	30	7.64
1000	7614	28	6.97	4374	30	7.71

spaces than for the scalar case as can be seen by comparing Tables 2.2 and 7.2. Similar reductions, however, are present for face-based coarse spaces as can be seen in Table 7.3. We note that the coarse space dimensions reported in column 2 of Table 7.2 are greater than 3 times the corresponding values in Table 2.2 because of the need for additional face-based constraints as discussed in §6.

Numerical results are also presented in Table 7.3 for the economic approach described in §6 whereby only three translational degrees are associated with some subdomain vertices. In other words, rotational degrees of freedom are not required for these vertices. This has the important effect of reducing the size of the coarse space. Notice in Table 7.3 that a significant reduction in the coarse space dimension n_c is achieved for the economic approach when compared with the standard approach. Remarkably, a reduction of about 5 times is achieved for larger numbers of subdomains for face-based coarse spaces. This reduction would asymptotically reach a factor of 6 as the number of subdomains increases.

7.1. Material Property Jumps. This example deals with a cubic domain decomposed into 64 smaller cubic subdomains and constrained on its left face. Three different distributions of material properties are considered as shown in Figure 7.1. The leftmost one has quasi-monotone face-connected paths, the middle one quasi-monotone edge-connected paths, and the rightmost one a checkerboard arrangement which is not covered by our theory.

The material properties in the white and blue regions are given by $\rho = 1$ for the scalar case and $E = 1$, $\nu = 0.3$ for elasticity. Likewise, the burnt orange and maize regions have $\rho = 10^3$, $E = 10^3$, and $\nu = 0.3$. Results for the scalar case and elasticity are shown in Table 7.4. Consistent with the theory, condition numbers for the scalar case grow sublinearly with respect to H/h for both face-connected and edge-connected paths. As expected, similar growth in condition numbers is observed for linear elasticity in the case of face-connected paths. We recall that the case of edge-connected paths is not covered by our theory for elasticity, and much larger condition numbers are apparent in the table. Remarkably, excellent results are obtained for the checkerboard arrangement of material properties for both the scalar case and linear elasticity when the originating BDDC coarse space is based on edges. Notice that the results for edge-connected and checkerboard properties are significantly poorer for face-based compared to edge-based coarse spaces for linear elasticity.

TABLE 7.3
Elasticity results for face-based coarse spaces. Coarse space dimension n_c and convergence results are shown for increasing numbers of subdomains N and fixed $H/h = 8$.

	face-based coarse spaces								
	standard approach			proposed approach			economic approach		
N	n_c	iter	cond	n_c	iter	cond	n_c	iter	cond
64	864	21	4.70	162	27	7.11	159	27	7.14
216	3240	22	4.90	750	27	7.01	669	27	6.93
512	8064	23	4.97	2058	28	7.06	1683	28	6.92
1000	16200	23	5.00	4374	28	7.07	3345	28	6.98

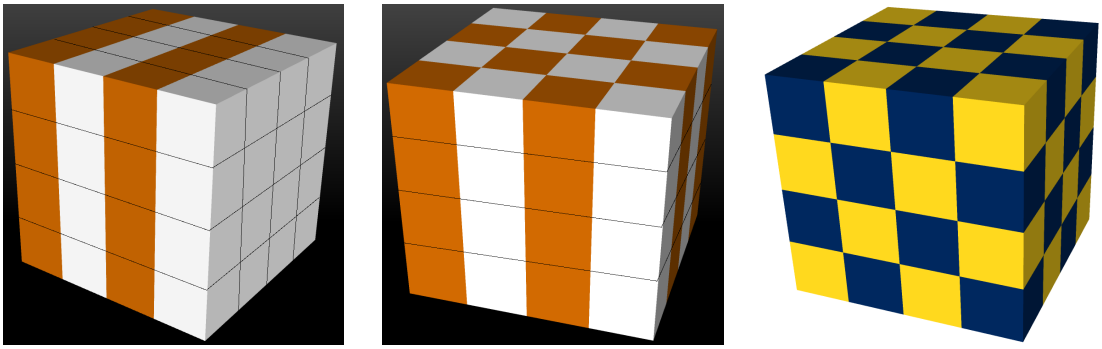

FIG. 7.1. *Material property distributions for a cube decomposed into 64 smaller cubic subdomains. The leftmost figure has quasi-monotone face-connected paths while the middle one only has quasi-monotone edge-connected paths. The rightmost figure shows a checkerboard arrangement of material properties.*

7.2. Unstructured Meshes and Decompositions. The next example considers two finite element models adapted from the Cubit [5] tutorial and shown in Figure 7.2. Results are shown in Table 7.5 for two different mesh resolutions of each model. Notice that the proposed approach again reduces the coarse space dimension without large increases in iterations. We note that the average number of elements per subdomain was chosen to be around 500, which is an order of magnitude smaller than what is not uncommon in practice. This was done to help reveal and correct shortcomings in how equivalence classes were made active in the coarse space.

7.3. Performance Comparisons. The benefits of the proposed approach become apparent when the number of subdomains is relatively large. The reason for this is that the cost for solving the coarse problem begins to dominate costs at the subdomain level. Thus, any reduction in the coarse space dimension can lead to reductions in overall solution times.

Results in Table 7.6 were obtained for a unit cube decomposed into N identical smaller cubic subdomains with 64 elements each using 64 cpus of a compute server. Although this is an unusually small number of elements per subdomain, it enables performance evaluations at large subdomain counts without the need for large computational resources. The table lists speedups using the proposed approach in both the initialization and solve phases for the iterative solution of the linear equations. Also shown in the table are results obtained using the economic approach for linear elasticity. As the number of subdomains increases, the relative amount of time spent in the coarse solver also increases. Here, edge-based and face-based coarse spaces were used for the scalar case and linear elasticity, respectively. Performance improvements are evident in the table, and the very favorable results for the economic approach suggest that it be studied further.

REFERENCES

TABLE 7.4
Results for the models in Figure 7.1.

scalar case												
	edge-based coarse spaces						face-based coarse spaces					
	face-connected		edge-connected		checkerboard		face-connected		edge-connected		checkerboard	
H/h	iter	cond	iter	cond	iter	cond	iter	cond	iter	cond	iter	cond
4	14	2.46	16	3.59	9	1.45	13	2.10	19	6.95	20	8.67
8	16	2.98	20	4.81	11	1.72	16	3.05	26	9.94	25	11.2
12	18	3.44	21	5.66	12	1.99	19	3.96	31	12.8	27	12.9
16	19	3.79	23	6.33	13	2.18	21	4.70	35	16.0	29	14.2
linear elasticity												
	edge-based coarse spaces						face-based coarse spaces					
	face-connected		edge-connected		checkerboard		face-connected		edge-connected		checkerboard	
H/h	iter	cond	iter	cond	iter	cond	iter	cond	iter	cond	iter	cond
4	25	6.03	40	72.3	24	6.57	26	7.03	68	1.5e3	52	192
8	33	10.9	53	112	32	11.1	34	12.1	94	2.0e3	66	299
12	38	14.5	61	135	36	14.4	40	16.0	112	2.2e3	75	348
16	42	17.4	68	152	38	16.9	44	19.3	124	2.3e3	80	378

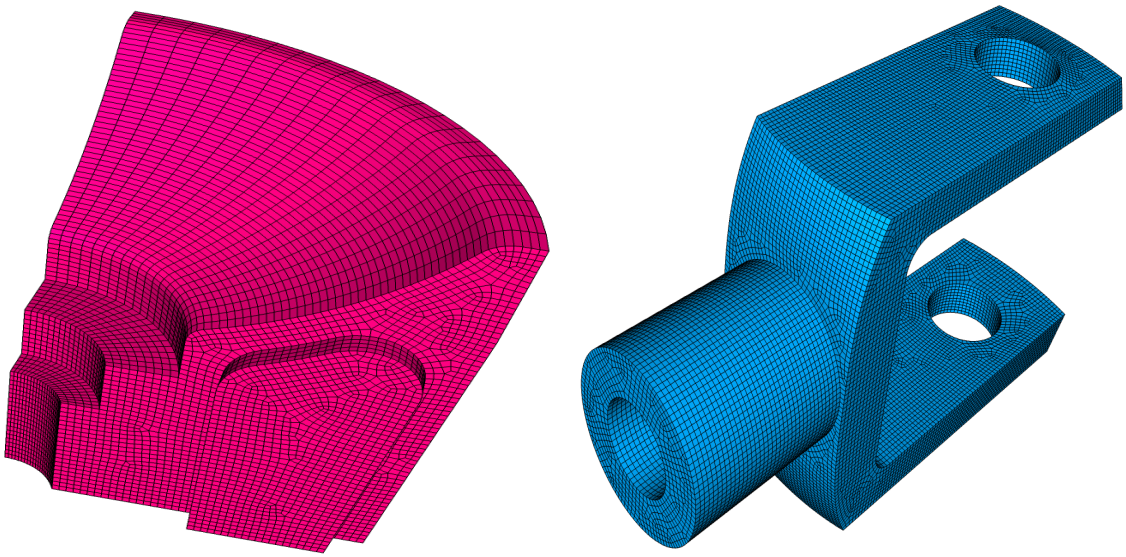

FIG. 7.2. *Two finite element models adapted from the Cubit [5] tutorial (model 1 on left, model 2 on right). Homogeneous essential boundary conditions are applied to the bottom and left of models 1 and 2, respectively.*

TABLE 7.5
Results for Models in Figure 7.2 and face-based coarse spaces. The number of subdomains and elements are denoted by N and nelem.

		scalar case						elasticity					
		standard approach			proposed approach			standard approach			proposed approach		
N	*nelem*	n_c	iter	cond	n_c	iter	cond	n_c	iter	cond	n_c	iter	cond
		Model 1											
100	47,887	376	27	9.52	236	34	16.6	2219	49	27.3	1416	62	54.5
805	363,024	3754	33	11.4	2909	43	19.3	22,096	62	41.3	17,454	85	122
		Model 2											
201	97,316	544	17	2.87	269	19	3.84	3246	30	8.26	1614	37	15.3
903	450,661	3543	17	3.00	2201	21	4.40	20,957	35	18.5	13,206	43	30.4

TABLE 7.6
Speedups in terms of the number of subdomains N and ratios of coarse space dimensions n_c.

	scalar case			elasticity					
	proposed			proposed			economic		
N	init	solve	ratio n_c	init	solve	ratio n_c	init	solve	ratio n_c
13,824	1.7	1.3	0.32	1.5	1.1	0.31	3.2	1.6	0.19
21,952	2.0	1.3	0.32	1.9	1.2	0.31	4.6	1.7	0.19
32,768	2.2	1.3	0.32	1.9	1.2	0.31	5.5	2.0	0.18
46,656	2.5	1.4	0.32	1.8	1.2	0.32	6.3	2.0	0.18

[1] S.C. Brenner and R. Scott: The Mathematical Theory of Finite Element Methods. Springer-Verlag, New York, Third edition (2008).

[2] S.C. Brenner and L.-Y. Sung. BDDC and FETI–DP without matrices or vectors. *Comput. Methods Appl. Mech. Engrg.*, **196**(8),1429–1435 (2007).

[3] E.T. Chung, H.H. Kim, and O.B. Widlund: Two-Level Overlapping Schwarz Algorithms for a Staggered Discontinuous Galerkin Method. SIAM J. Numer. Anal. **51**(1), 47–67 (2013).

[4] P.G. Ciarlet: *Linear and Nonlinear Functional Analysis with Applications.* SIAM, 2013.

[5] T. Blacker, S.-J. Owen, and et al. *CUBIT, Geometry and Mesh Generation Toolkit, 15.3 User Documentation.* Sandia National Laboratories, Albuquerque, New Mexico and Livermore, California, July 2017. SAND2017-6895 W.

[6] C.R. Dohrmann: A preconditioner for substructuring based on constrained energy minimization. SIAM J. Sci. Comput. **25**(1), 246–258 (2003).

[7] C.R. Dohrmann: An approximate BDDC preconditioner. Numer. Linear Algebra Appl. **14**(2) 149–168 (2007).

[8] C.R. Dohrmann and O.B. Widlund: On the design of small coarse spaces for domain decomposition algorithms. SIAM J. Sci. Comput. **39**(4), A1466–A1488 (2017).

[9] M. Dryja, M.V. Sarkis, and O.B. Widlund: Multilevel Schwarz methods for elliptic problems with discontinuous coefficients in three dimensions. Numer. Math. **72**(3), 313–348 (1996).

[10] C. Farhat, M. Lesoinne, and K. Pierson. A scalable dual-primal domain decomposition method. *Numer. Lin. Alg. Appl.*, **7**(7–8), 687–714 (2000).

[11] C. Farhat, M. Lesoinne, P. Le Tallec, K. Pierson, and D. Rixen. FETI-DP: A dual-primal unified FETI method – part I: A faster alternative to the two-level FETI method. *Internat. J. Numer. Methods Engrg.*, **50**, 1523–1544 (2001).

[12] M.A. Heroux and J.M. Willenbring. Trilinos Users Guide. Technical Report SAND2003-2952, Sandia National Laboratories, 2003.

[13] A. Heinlein, A. Klawonn, O. Rheinbach, and O.B. Widlund: Improving the Parallel Performance of Overlapping Schwarz Methods by Using a Smaller Energy Minimizing Coarse Space. Proceedings of the twenty-fourth International Conference on Domain Decomposition held in Svalbard, Norway, February 6–10, 2017.

[14] G. Karypis, R. Aggarwal, K. Schoegel, V. Kumar, and S. Shekhar: METIS home page, http://glaros.dtc.umn.edu/gkhome/views/metis.

[15] A. Klawonn and O. Rheinbach. Robust FETI-DP methods for heterogeneous three dimensional linear elasticity problems, Comput. Methods Appl. Mech. Engrg. **196**(8), 1400–1414 (2007).

[16] A. Klawonn and O. Rheinbach: Inexact FETI-DP methods. *Internat. J. Numer. Methods Engrg.*, **69**(2):284–307, 2007.

[17] A. Klawonn, O.B. Widlund, and M. Dryja: Dual-primal FETI methods for three-dimensional elliptic problems with heterogeneous coefficients. *SIAM J. Numer. Anal.*, **40**(1), 159–179 (2002).

[18] A. Klawonn, O. Rheinbach, and O.B. Widlund: An analysis of a FETI–DP algorithm on irregular subdomains in the plane. SIAM J. Numer. Anal. **46**(5), 2484–2504 (2008).

[19] A. Klawonn and O.B. Widlund: Dual-Primal FETI methods for linear elasticity. Comm. Pure Appl. Math. **59**(11), 1523–1572 (2006).

[20] A. Klawonn, O.B. Widlund, and M. Dryja: Dual-primal FETI methods with face constraints. Recent developments in domain decomposition methods Held in Zürich, June 7–8, 2001. L.F. Pavarino and A. Toselli, (eds). Springer Lect. Notes Comput. Sci. Eng. **23**, 27–40 (2002).

[21] J. Li and O.B. Widlund. FETI–DP, BDDC, and Block Cholesky Methods. *Internat. J. Numer. Methods Engrg.*, **66**(2), 250–271 (2006).

[22] J. Li and O.B. Widlund: On the use of inexact subdomain solvers for BDDC algorithms. Comput. Methods Appl. Mech. Engrg. **196**(8), 1415–1428 (2007).

[23] J. Mandel and C.R. Dohrmann: Convergence of a Balancing Domain Decomposition by Constraints and Energy Minimization. Numer. Linear Algebra Appl. **10**(7), 639–659 (2003).

[24] J. Mandel, C.R. Dohrmann, and R. Tezaur: An algebraic theory for primal and dual substructuring methods by constraints. Appl. Numer. Math. **54**(2), 167–193 (2005).

[25] J. Mandel, B. Sousedík, and C.R. Dohrmann: Multispace and multilevel BDDC. Computing **83**(2-3), 55–85 (2008)
[26] L.F. Pavarino, S. Scaccchi, O.B. Widlund, and S. Zampini: Isogeometric BDDC deluxe preconditioners for linear elasticity. Math. Mod. Meth. Appl. Sci. **28**(7), 1337–1370 (2018).
[27] J. Toivanen, P. Avery, and C. Farhat: A multi-level FETI-DP method and its performance for problems with billions of degrees of freedom. Int. J. Numer. Methods Eng. **116**, 661–682 (2018).
[28] A. Toselli and O.B. Widlund: Domain Decomposition Methods - Algorithms and Theory, *Springer Series in Computational Mathematics*, **34**. Springer-Verlag, Berlin Heidelberg New York (2005).
[29] X. Tu: Three-level BDDC in Two Dimensions. Internat. J. Numer. Methods Engrg., **69**(1), 33–59 (2007).
[30] X. Tu: Three-level BDDC in Three Dimensions. SIAM J. Sci. Comput. **79**(4), 1759–1780 (2007).
[31] O.B. Widlund and C.R. Dohrmann: Small coarse spaces for overlapping Schwarz algorithms with irregular subdomains. Proceedings of the twenty-fourth International Conference on Domain Decomposition held in Svalbard, Norway, February 6–10, 2017.